Engineering Steels at the Nanoscale for Improved Performance

Peter D Hodgson[1], Ilana B Timokhina[1], Hossein Beladi[1], Thomas Dorin[1], Nicole Stanford[2] and Minghui Cai[1]

[1]Institute for Frontier Materials, Deakin University,
Geelong, VIC 3217
Phone: (61) 0418501266
Email: peter.hodgson@deakin.edu.au

[2]Materials Engineering Department, Monash University, Melbourne, VIC 3800

INTRODUCTION

Steel is often seen as an old fashioned structural material that will be replaced by newer lighter weight, higher performance materials. This has been the case for my entire career in the industry; which now spans 35 years. Plastics, composites, aluminium and magnesium have all at various times been seen as replacements for steel in the automotive and other sectors.

What has not been factored into these projections is that steel companies will continue to innovate and develop new property packages which on a cost basis cannot be met by other materials. Even some of the most expensive potentially high volume steels, such as TWIP steels, are still a small fraction of the price of composites. That being said it is likely that the future of the automotive sector will be to develop hybrid material solutions as in the coming decade weight reduction will no doubt push the limit for steels.

This paper considers a range of options for engineering steels at the ultrafine, nanoscale and even atomic level. This is now possible because we have the analytical tools to characterise steels at these various length scales and through this understanding we can then engineer the microstructure to achieve the required properties.

This paper is dedicated to the memory of Professor Keith Brimacombe who always drew the link between excellent fundamental research that was linked to practical, real world solutions. This bridge was often through both advanced experimentation as well as models, an approach we strongly believe in. In the following sections we will explore the development of microstructure over the various length scales and how this may provide alloys for the future. Also new compact, low energy processes, such as strip casting, and the development of new microstructures and precipitation reactions are considered. Not all of this work is ready for industrial application but it does point to new directions in steel development and highlights the potential to still engineer steel at the nanoscale to achieve improved properties.

RESULTS AND DISCUSSION

Limits of ultrafine ferrite

Grain refinement through austenite to ferrite transformation is generally obtained by the enhancement of ferrite nucleation density and/or reducing its growth rate. The deformation of austenite in the non-recrystallization region significantly alters the extent of ferrite nucleation and growth rate through three means. Firstly, it roughens the austenite grain boundary due to the interaction of slip system with the boundary, enhancing ferrite nucleation sites. Secondly, the deformation induces intergranular defects, which are mostly suitable for ferrite nucleation. Lastly, it limits the ferrite growth through reducing the gap between austenite grain boundaries. Therefore, the enhancement of deformation leads to a progressive ferrite grain refinement. However, a limiting ferrite grain size of 5 μm exists using the conventional controlled thermomechanical processing, regardless of the retained strain.

In the early 1990s, it was shown that the ferrite coarsening takes place during ferrite transformation, leading to a significant decrease in the apparent nucleation density [1]. The extent of ferrite coarsening appears to reduce as the retained strain increases and similarly depends on cooling rate and steel composition. In other words, the parameters, which enhance the full impingement of ferrite grains at an early stage of transformation, significantly limit the coarsening phenomenon, leading to extreme grain refinement.

To overcome this barrier, different thermomechanical approaches were developed over last few years to further reduce the ferrite grain size to ~1 μm. One of the most popular and compatible approaches to the industrial scale is dynamic strain-induced transformation (DSIT). In this approach, the strain is applied between the Ae3 and Ar3 temperatures, leading to the transformation of metastable austenite to ferrite during straining [2]. This results in a significant grain refinement to the order of 1 μm, potentially doubling the strength compared with the conventional rolling process (i.e. 5 μm) (Figure. 1 a).

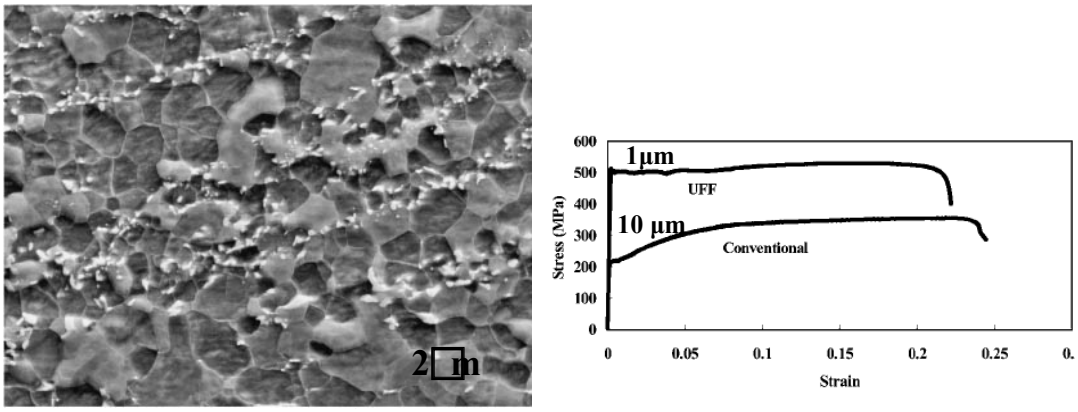

a b

Figure 1. (a) Ultrafine ferrite microstructure consisting of fine ferrite grains and cementite formed through DSIT process in 1020 plain carbon steel and (b) stress-strain curves of fully ferritic microstructure with different grain sizes [10].

It was believed that the simultaneous deformation and transformation enhances the full impingement of fine ferrite grains at an early stage of transformation, limiting the coarsening phenomenon. This comparatively simple approach can be employed for a wide range of steel composition [3]. However, this requires a large strain at a relatively low temperature regime to form an optimum volume fraction fine ferrite grains during deformation. This issue was successfully overcome through building and maintaining fine ferrite grains (i.e. controlling the coarsening) over a number of pass strains [4,5]. This approach is potentially applicable in more conventional rolling mills. Large-scale laboratory and industrial trails were performed in China [6] and Korea [7], where very fine ferrite grain size was produced through tight control over temperature and deformation. However, the grain size was close to 3 μm. In Japan, multiple deformations followed by immediate water-quenching after the last stand was employed, leading to the dual phase bulk product consisted of ultrafine ferrite grain size close to 1 μm and martensite islands [8].

The strength of ultrafine ferrite microstructure reveals a significant increase in comparison with the coarse ferrite grained structure (Figure 1 b), as predicted by Hall-Petch relationship. However, most of the ultrafine ferrite steels produced to date suffer from low work-hardening rate and a yield strength that approaches the value of the tensile strength (i.e. producing a flat flow curve, Figure 1 b). In other words, they mostly have a high yield ratio (lower yield stress/ultimate tensile stress) in a range of 0.7-1 [9] (Figure 1 b), whereas the ratio is closer to 0.7 in conventional structural steels.

This undesired mechanical property motivates the search for novel microstructures to improve the work-hardening rate of this class of steels. The most common approach is to induce a second phase such as martensite in the ultrafine microstructure. The presence of martensite islands in a UFF structure significantly decreases the yield ratio to ~0.6-0.7, though the continuous yielding phenomena (i.e. low yield strength and high work-hardening rate, Figure 2) [10].

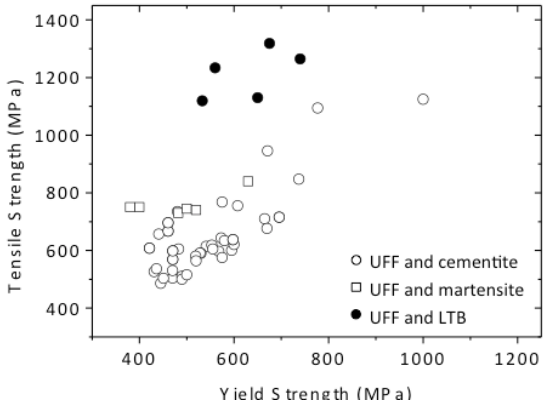

Figure 2. Ultimate tensile strength vs yield strength for different UFF and second phase microstructures [13].

Bainite was also induced in the UFF microstructure as a second phase since it offers higher toughness. More recent bainite structure development in advanced transformation-induced plasticity (TRIP) steels revealed that the transformation of bainite at relatively low temperature (150-350°C) leads to nanosize bainitic laths and retained austenite films, known as nanobainitic steels (which are described in more detail in the next section). These nanostructured bainitic steels are mainly produced in highly alloyed steels (0.79C–1.5Si–1.98Mn–0.98Cr–0.24Mo–1.06Al–1.58Co wt.%), designed based on a thermodynamic approach, and offer unique combinations of mechanical properties [11, 12].

Ultrafine and nano-bainite

To enhance the work-hardening behaviour of UFF microstructure further, a novel thermomechanical approach was recently developed to produce a unique microstructure that consisted of fine ferrite grains along with low temperature bainite in a relatively low carbon low alloy steel [13]. The alloy was designed so that it provides a moderate hardenability. This enables deformation of austenite at a relatively low temperature of 570°C followed by reheating to the ferrite transformation regime (650°C) where it was held to form the maximum ferrite volume fraction before the precipitation of carbides. The deformation enhances the ferrite nucleation sites and the low temperature ferrite transformation limits the coarsening of ferrite grains. Consequently, the warm-deformed austenite partially transformed to carbide-free fine ferrite grains. Indeed, the partial transformation of austenite results in the carbon-enrichment of the remaining austenite, reducing its Bs and Ms transformation temperatures. Consequently, the remaining austenite was transformed into low temperature bainite (i.e. at 200-350°C), resulting in a unique microstructure consisting of fine ferrite grains in conjunction with a low temperature bainite second phase (Figure 3 a). This class of steel further improved the work-hardening behavior, leading to a yield ratio of 0.45-0.6. While this is not a commercially viable process it informs our understanding of the formation of ultrafine microstructures and the role of second phase. An important aspect of this is that we were able to show that you can have static transformation to an ultrafine microstructure, whereas previous work suggested the need for it to occur dynamically. The real need is to setup the initial austenite microstructure to have a high density of nucleation sites for ferrite formation. This is still a challenge for industrial processes.

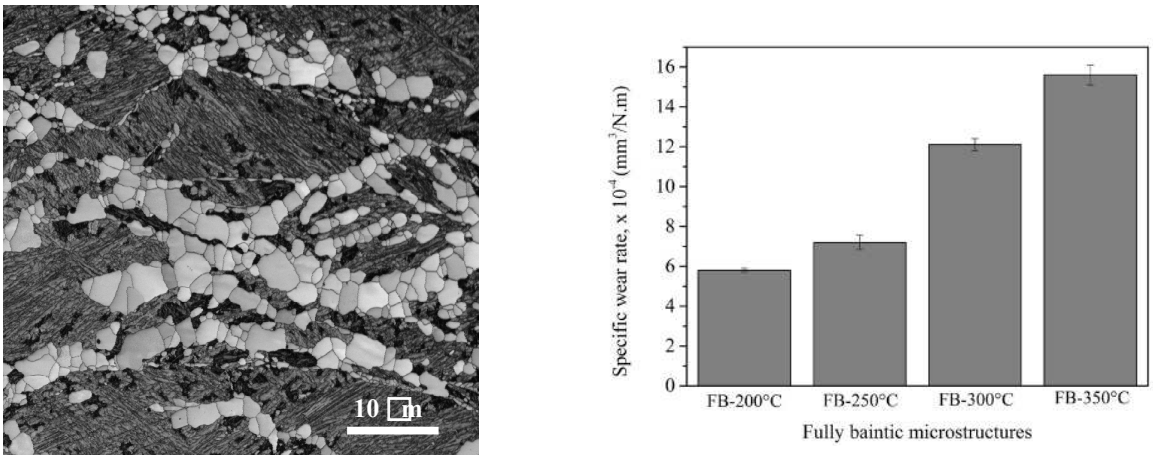

a b

Figure 3. The microstructure of fine ferrite in conjunction with low temperature bainite [13] (a) and the specific wear rate for different nano-bainitic steels subjected to two-body abrasion environment (b).

Wear behaviour of nanobainitic steels

The unique properties of nanobainitic steels make them good candidates for heavy industries such mining, where the steel is subjected to a severe environment. In our recent study, the two-body abrasive wear resistance was studied in nanostructured bainitic steel formed at different transformation temperatures (200-350°C). The fully bainitic microstructures largely consisted of bainitic ferritic laths and retained austenite. The bainitic phase transformation significantly influenced the characteristics of the microstructural constituents (i.e. size, morphology, carbon content and volume fraction). The retained austenite morphology changed from film to film+blocky with an increase in the transformation temperature. The wear resistance was greatly enhanced with a decrease in the transformation temperature due to the refinement of microstructure constituents (i.e. greater hardness) and the extent of the retained austenite TRIPing (TRansformation Induced Plasticity) phenomenon. The presence of coarse and blocky retained austenite in high transformation temperature bainitic microstructures significantly reduced their mechanical stability. This led to an early onset of the TRIP effect during the two-body abrasive wear testing, resulting in the formation of coarse martensite. The fresh martensitic region was more vulnerable to crack initiation and propagation due to its irregular morphology compared with the fresh martensite formed from the thin film retained austenite at low transformation temperatures (i.e. nanobainitic microstructures). Ultimately, this resulted in higher material loss with an increase in the phase transformation temperature (Figure 3 b).

Ultrafine ferrite grains produced by asymmetric rolling (ASR)

An increase in the mechanical properties of metals may be obtained by ASR. The main advantage of ASR is that it can introduce homogeneous simple shear through the thickness of the sheet. Such a shear increases the efficiency of grain refinement, rotates the rolling texture, and increases the yield and ultimate tensile strengths. The effect of ASR on the microstructure of the steel plate with the composition of 0.12C-1.35Mn-0.49Si-0.02Ni-0.014Cr-0.02Cu-0.035Nb-0.019Ti-0.037N (wt. %) has been recently investigated by our group. The microstruture of the as-received material consists of coarse-grained ferrite with a ~25 μm grain size and ~10% pearlite. The initial texture of this material in Figure. 4 b**,** exhibited dominant hot rolling textures with a ε-fiber ⟨110⟩//TD (~43.6%) and γ-fiber ⟨111⟩//ND (~26.8%) with a maximum intensity of 2.0 multiples of a random distribution (MRD).

Microstructural investigation on both AsR and SR samples after 50% rolling and water quenching (Figure 4) reveals that both exhibited UFG ferrite grains with small amounts of martensite of 4-10% (white regions). Shear deformation bands were clearly observed at the center layer for the AsR sample (Figure 4 c), which is totally different from the nearly uniform distribution of ferrite grains at the center layer of the SR sample (Figure 4 a). According to the partitioned microstructures, the fractions of dynamic ferrite were estimated to be approximately 58~68% and 44~61%, for the AsR and SR samples, respectively. This indicates that a relatively large amount of warm-rolled ferrite was still observed, which is thought to be probably related to the temperature gradients between the surfaces of high-temperature specimens and cold working rolls as well as decarburisation during reheating [14, 15].

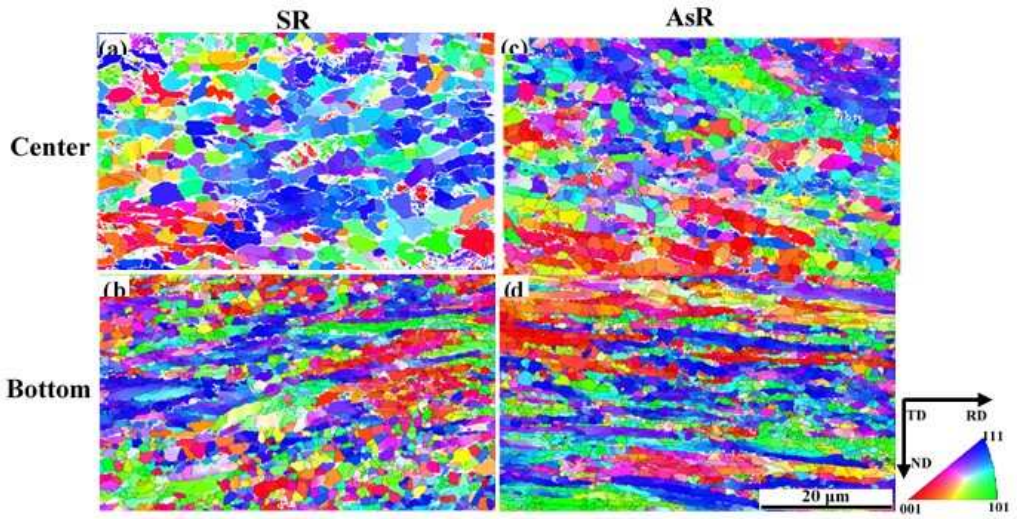

Figure 4. Inverse pole figure (IPF) colouring maps for (a, b) SR and (c, d) AsR samples after 50% rolling at 800°C and water quenching. The bottom surface layer corresponds to the surface close to the large working roll. White regions represent martensite, which was distinguished from ferrite by its significant low Band Contrast (BC) values. RD, TD and ND refer to rolling, tangential and normal directions, respectively.

A significant difference in grain size distribution between the center layers of AsR and SR samples implies a more efficient grain refinement process during asymmetric rolling, due to large equivalent strains resulting from a compressive strain and additional shear deformation. Specifically, the average grain size of AsR can reach as fine as 0.92-1.09 μm throughout the sheet thickness. The inhomogeneous duplex structure gradient in the UFG ferrite was thought to increase the capacity of the microstructure to accommodate the plastic stability during tensile deformation, which could be very beneficial for maintaining the tensile plasticity to a large strain concurrent with pronounced strain hardening [14, 15].

After 75% asymmetric hot rolling at 800 °C, the through-thickness gradient microstructure (Figure 5 a) exhibited ultrafine/sub-micron ferrite grains with an average grain size of ~1.06± 0.72 μm and some amount of martensite (dark regions), and the ferrite grain size distribution was clearly illustrated in Figure 5 b. The ferrite grain size was refined as fine as a few hundreds of nanometers near the large roll surface, and gradually increased with the sheet thickness to 2~3 μm at the layer of the small roll surface (Figure 5 c). The gradient structure provided a unique opportunity for revealing the instrinsic tensile plasticity of ultrafine ferrite without strain localization.

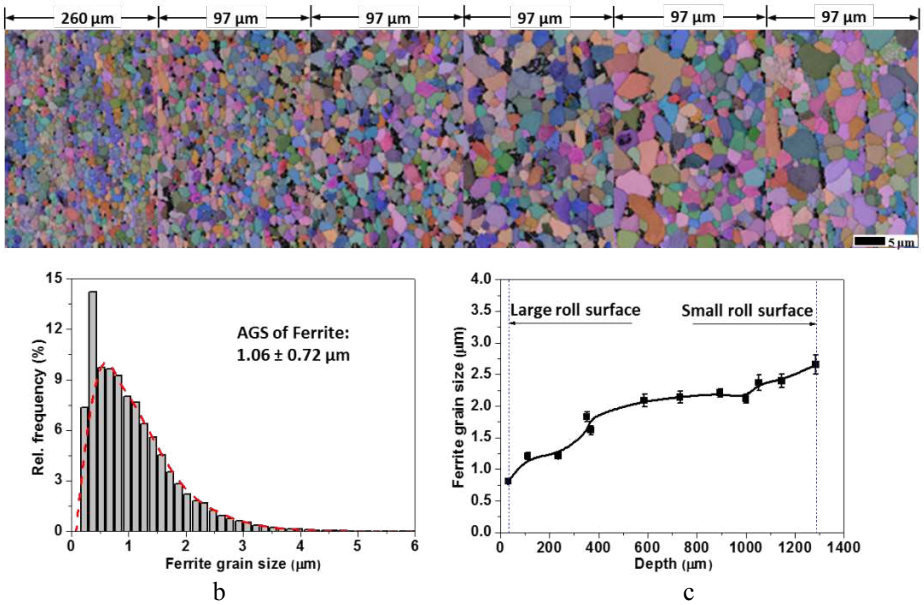

Figure 5. Ultrafine or sub-micron ferrite grains gradient throughout the sheet thickness (final thickness: ~1.3mm); (b) ferrite grain size distribution; (c) change in ferrite grain size as a function of the sheet thickness.

Ultrafine ferrite/austenite duplex microstructure produced by reverse transformation of the deformed martensite.

A steel with a composition of Fe-0.167C-6.57Mn-1.1Al-0.05Nb-0.22Mo-0.03N (wt.%) was used to produce an UFG microstructure. A comparison of Figure 6 clearly demonstrates the formation process of ultrafine ferrite grains from the deformed martensite during isothermal holding by means of the following possible sequences: (i) the original martensitic laths with thickness 100-200 nm underwent intense plastic deformation, and subdivided into finer crystals with high dislocation density; (ii) the martensitic structure was recovered through dislocation rearrangement during annealing, resulting in the formation of sub-grains or boundaries; and (iii) with further recovery and recrystallization, more and more sub-boundaries were turned into clear boundaries, resulting in the formation of new UFG grains with HAGBs [16, 17].

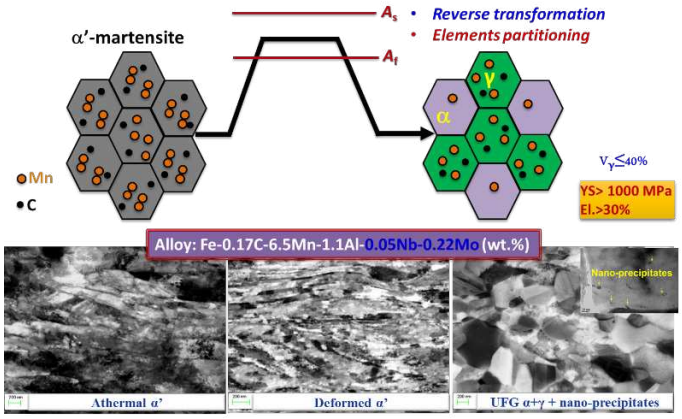

Figure 6. Microstructure evlotion during hot rolling, 75% cold rolling and intercritical annealing at 650 ^{o}C for 30 min, and a schematic illustration of elements partitioning during reverse transformation.

Cluster/nano-precipitation hardening

The formation of solute clusters, along with interphase nano-precipitates in an Fe–0.03C–1.5Mn–0.2Si–0.29Cr–0.22Mo–0.05Ti–0.025Al wt.% steel formed during austenite to ferrite transformation, has recently been extensively studied by the current authors using Atom Probe Tomography (APT) [18, 19]. It was shown that as the size of the cluster/nano-particles increased, the composition range became narrower; reducing the residual Fe and, finally, the cluster composition approached that of MC carbide [19]. In order to study the changes in composition of clusters during their nucleation and growth, the experimental program of interrupted isothermal treatments at 650^{o}C for 1200 and 1700 s was designed. It was proved by HR TEM and INLO APT that at the beginning of transformation after 1200 s only clusters were formed (Figure 7). However, the clusters were not randomly redistributed within the ferrite matrix but aligned along the parallel lines with a regular spacing of 10±0.2 nm between these lines and a distance between the clusters in the row of 6.5±0.5 nm. It is likely that these clusters were nucleated at the interface as the transformation front moves through the austenite. The composition of clusters varied between 37 – 73 C and 24 - 53 Ti at.%.

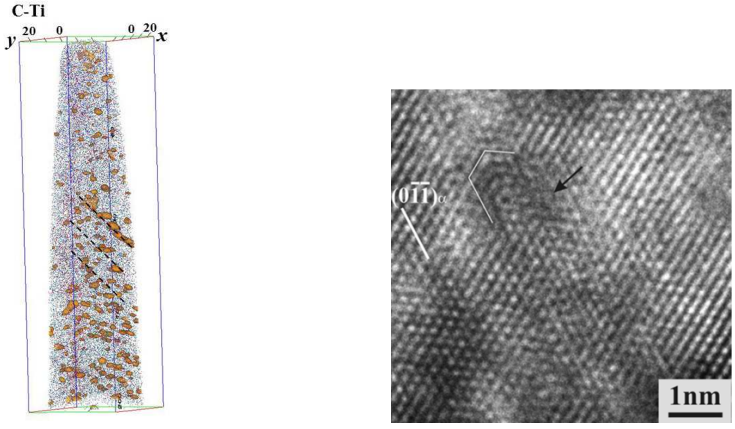

a b

Figure 7. C-Ti atom map (a) and HR TEM micrograph of clusters (b) formed after 1200s of isothermal hold.

It is important to highlight here, that Mo was not present in the composition of clusters after this isothermal treatment. The nano-precipitates were observed at later stages of precipitation after 1700 s of transformation. The nano-precipitates were aligned along the parallel lines with a regular spacing of 17±1 nm, which is a larger distance than after 1200 s. The newly formed nano-precipitates formed after 1700 s followed a crystallographic orientation relationship of a Baker-Nutting with the ferrite matrix (Figure 8) leading to the greater coherency that precipitates adopt with ferrite when they precipitate at the ferrite/austenite interface. The composition of the nano-precipitates after 1700 s hold had 17 ± 5 Mo as long as 56 ± 5 C, 24 ± 8 Ti at.%, i.e. Ti was partially replaced by Mo. It is suggested that at low austenite to ferrite transformation temperature as 650^{o}C, the transformation of austenite to ferrite is accelerated at the beginning of transformation because of large driving force, i.e. the ledge mobility is high and only clusters were formed, whereas at the late stages, the transformation is retarded that allows the nano-precipitate formation. It appeared that since the mobility of the interface within the first 1200s of isothermal hold at 650^{o}C is fast and there is no time for the nucleation and growth of the interphase precipitates and only nucleation of clusters occurred. What needs to be emphasized here is that the size of the particles was similar after 1200 and 1700 s of isothermal hold, which contradicts results reported earlier [20] that the size of interface precipitation carbides in inversely proportional to the ledge mobility.

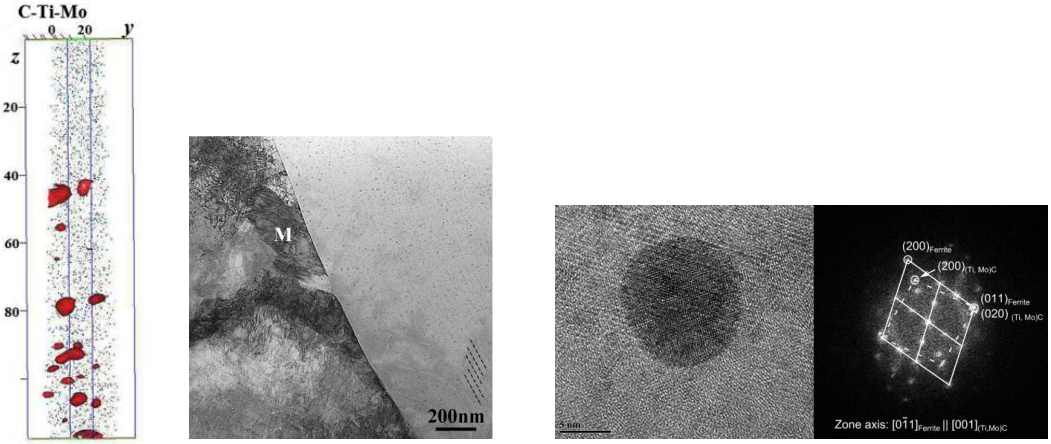

a b

Figure 8. C-Ti-Mo atom map (a) and HR TEM micrograph of nano-particles (b, c) formed after 1700s of isothermal hold.

Another type of the particles which were formed along the grain boundary was also observed. They showed the equilibrium composition of MC (Figure 9).

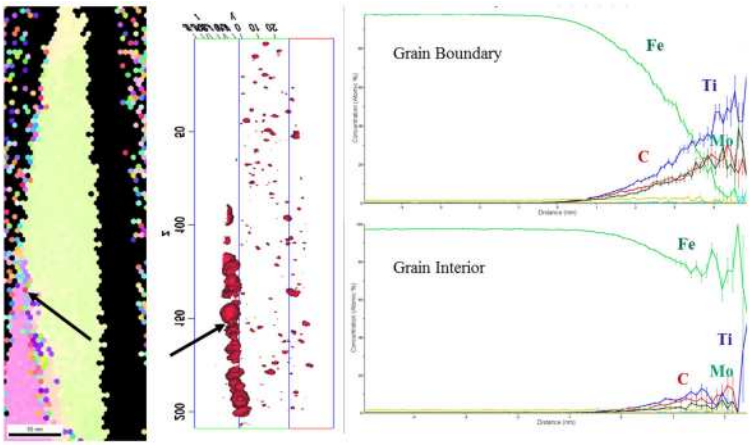

a b

Figure 9. The EBSD map (a), the APT iso-surface of the particles formed in the matrix and at the grain boundary pointed by the arrows (b), and compositional profile across the particle at the grain boundary and in the matrix.

Another research question was if it is possible to increase the precipitation hardening by increasing the level of strain from 0.3 to 1 at the deformation temperature of 890^{o}C. An increase in the amount of strain decreased the distance between the

rows only after 0.3 strain, and after that the distance remained the same (Figure 10). The distance between the precipitates remained similar up to a strain of 1 and then reduced after a strain of 1 (Figure 10). The average number density of the nano-precipitates increased with increasing the strain (Figure 10).

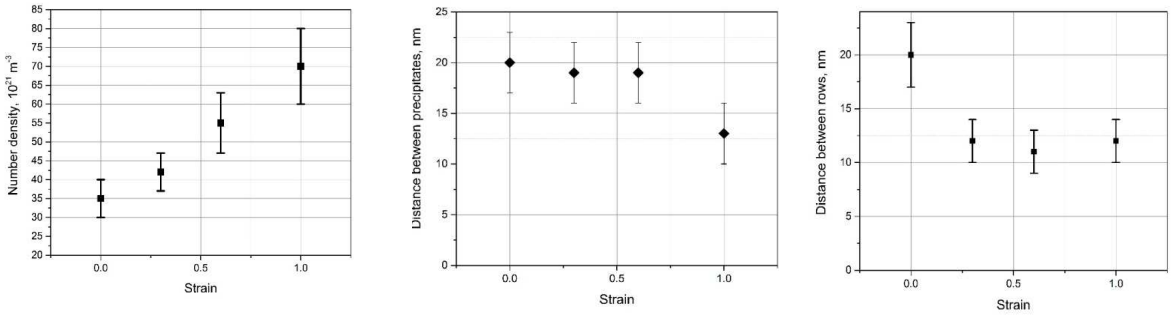

Figure 10. The effect of strain on the interphase precipitation.

Precipitation hardening of low alloy steel during direct strip casting

Direct strip casting is a novel energy efficient manufacturing technology [21]. This continuous casting process involves first the rapid solidification of steel and then the coiling of the metal sheet. The extremely rapid cooling rate involved has been shown to result in supersaturated microstructures [21]. The formation of precipitates occurs during the coiling process and as such it is critical to optimise the temperature and duration of coiling. In our recent study, the precipitation is investigated in a low carbon low niobium steel (Fe-0.11C-0.16Nb-0.59Mn-0.16Si wt.%) produced via direct strip casting. The steel samples were produced on a lab-scale apparatus known as a dip tester. During dip testing, a Cu substrate is rapidly immersed into a pool of liquid steel and which simulates the rapid solidification encountered during direct strip casting. Coiling is then simulated by rapidly transferring the as-cast specimen into a furnace set at the coiling temperature. In this study, coiling was performed in the ferrite phase field at 600 ^{O}C [22]. Under these casting conditions, the ferrite classically exhibit a bainitic morphology, Figure 11.

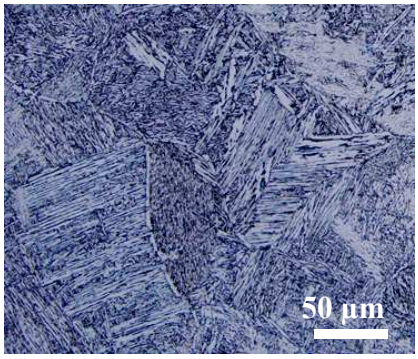

Figure 11: Micrograph of an as-cast sample.

Transmission electron microscopy revealed that no precipitates were present in the as-cast sample with no coiling, Figure 12 (a). This observation confirms that the direct strip casting process results in a supersaturated microstructure. By contrast, the sample coiled for 10000s at 600 ^{O}C exhibited small homogeneously distributed precipitates, Fig. 12 (b). APT is necessary to fully identify the composition of these precipitates, Figure 13. A significant number of precipitates could be identified in APT and they were found to contain ~80%Fe.

The typical Small angled neutron scattering (SANS) patterns of a sample free from precipitates and an aged sample that contains precipitates are displayed in Figure 14. The SANS patterns contain a nuclear and a magnetic contribution to scattering. By integrating these pattern, following the method described in [24], the size of the precipitate can be obtained. In the present case, the average precipitate diameter after 10000 s at 600 ^{O}C was found to be 3.6 nm. The scattering contrast from the precipitates depends on their exact composition and hence it is necessary to know the precipitate composition to quantitatively measure their volume fraction with SANS.

The composition obtained with the APT, Figure 13, can be used to quantitatively obtain the volume fraction of these precipitates. In the present case, the volume fraction after 10000 s at 600 ^{O}C was found to be 0.4%. This volume fraction is higher than the equilibrium volume fraction considering a stoichiometric composition of $Nb(C_{0.5},N_{0.5})$ [24]. The reason for this high value is due to the high Fe content inside the precipitates as shown with the APT.

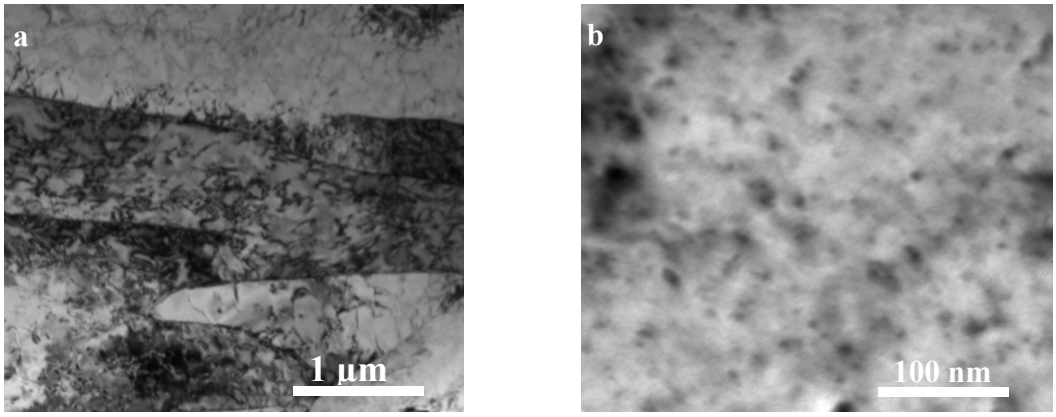

Figure 12: TEM of (a) an as-cast sample and (b) a sample coiled for 10000 s at 600 ^{O}C.

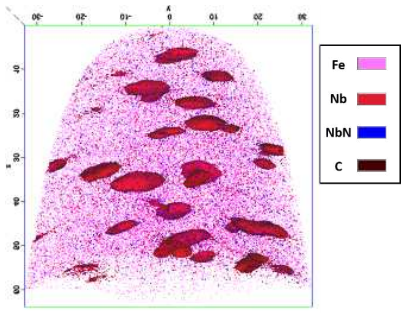

Figure 13: APT reconstructed dataset of a sample coiled 10000 s at 600 ^{O}C.

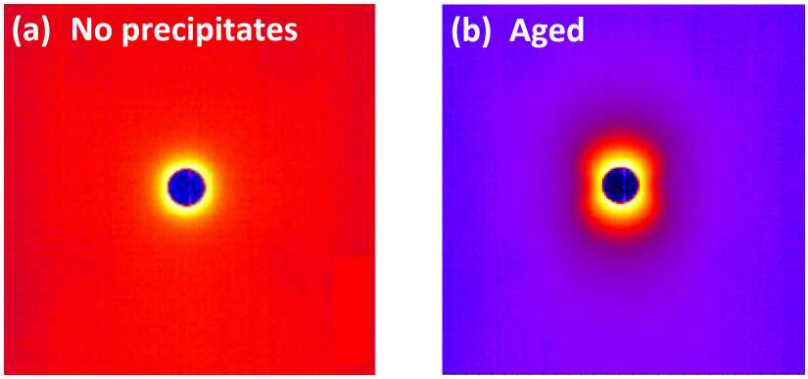

Figure 14. SANS pattern of (a) a sample with no precipitates and (b) an aged sample that contains precipitates

We suggest that the understanding the formation kinetics of precipitates in metallic systems is critical and can then be used to optimise the precipitate distribution that will yield optimal mechanical properties of the obtained steel.

SUMMARY

The present work has demonstrated that steels continue to evolve to compete with other lightweight materials, especially for automotive applications. There are many different approaches to improving the strength- ductility combination of steels and

in the current review the focus has been on developing and understanding ultrafine and nanostructures in steel. This has been supported by the ongoing development of high throughput and high resolution characterisation techniques that allow us to develop enhanced understanding of these microstructures and their evolution.

ACKNOWLEDGMENTS

Much of this work was funded by the Australian Research Council and in particular the authors want to acknowledge the support for the ARC Laureate Fellowship of PDH.

REFERENCES

1. R. Priestner, P.D. Hodgson, Mater. *Sci. Technol.,* Vol. 8, 1992, pp. 849-854.

2. P.D. Hodgson, M.R. Hickson, R.K. Gibbs, *Strain-induced transformation of ultrafine microstructure in steel*, United State Patent No. 6,027,587, 2000.

3. M.R. Hickson, R.K. Gibbs, P.D. Hodgson, *ISIJ Int.*, Vol. 39, 1999, pp. 1176-1180.

4. G.L. Kelly, H. Beladi, P.D. Hodgson, *ISIJ Int.*, Vol. 42, 2002, pp. 1585–1590.

5. H. Beladi, G.L. Kelly, P.D. Hodgson, *Metall. Mater. Trans. A*, Vol. 38, 2007, pp. 450–463.

6. H. Dong, X. Sun, W. Hui, S. Zhang, J. Shi, M. Wang, *ISIJ Inter.*, Vol. 48, 2008, pp. 1126-1132.

7. H.C. Lee, K.K. Um, *ISIJ Inter*., Vol. 48, 2008, pp. 1050-1055.

8. K. Miyata, M. Wakita, S. Fukushima, M. Eto, T. Sasaki, T. Tomida, *Mater. Sci. Forum,* Vol. 539-543, 2007, pp. 4698-4703.

9. H. Beladi, G.L. Kelly, P.D. Hodgson, *Int Mater Rev*, Vol. 52, 2007, p. 14.

10. P.D. Hodgson, *Mater Forum*, Vol. 23, 1999, p. 105.

11. H.K.D.H. Bhadeshia, *Mater Sci Technol*, Vol. 21, 2005, p. 1293.

12. F.G. Caballero, H.K.D.H. Bhadeshia, K.J.A. Mawella, D.G Jones, P Brown, *Mater Sci Technol*, Vol. 17, 2001, p. 512.

13. H. Beladi, I.B. Timokhina, X.Y. Xiong, P.D. Hodgson, *Acta Mater,* Vol. 61, 2013, pp. 7240-7250.

14. M.H. Cai, X. Wei, B. Rolfe, P.D. Hodgson, *Materials Science and Engineering A*, Vol. 641, 2015, pp. 297-304.

15. M.H. Cai, S. Singh Dhinwal, Q.H. Han, Q. Chao, P.D.Hodgson, *Materials Science and Engineering A*, Vol. 583, 2013, pp. 205-209.

16. M.H. Cai, W.J. Zhu, N. Stanford, L.B. Pan, Q. Chao, P.D. Hodgson, *Materials Science and Engineering A*, Vol. 653, 2016, pp. 35-42.

17. M.H. Cai, Z. Li, Q. Chao, P.D. Hodgson, *Mater. Metall. Trans. A*, Vol. 45, 2014, pp. 5624-5634.

18. I. Timokhina, P. Hodgson, S. Ringer, R. Zheng, E. Pereloma, *Scripta Materialia*, Vol. 56, 2007, pp. 601-603.

19. S. Mukherjee, I.B. Timokhina, C. Zhu, S.P. Ringer, P.D. Hodgson, *Acta Materialia*, Vol. 61, 2013, p. 2521.

20. R.W.K. Honeycombe, "Transformation from austenite in alloy steels", *Metall. Mater. Trans*., Vol. 7, 1976, pp. 915-935.

21. M. Ferry, *Direct Strip Casting of metals and alloys*, Woodhead Publishing, 2006.

22. T. Dorin, N. Stanford, A. Taylor and P. Hodgson, *Met. Mat. Trans. A,* Vol. 46A, 2015, pp. 5561-5571.

23. T. Dorin, K. Wood, A. Taylor, P. Hodgson and N. Stanford, *Under review,* 2016.

24. T. Dorin, K. Wood, A. Taylor, P. Hodgson and N. Stanford, *Mat. Char.,* Vol. 112, 2016, pp. 259-268.